Chapter-II

Synthesis and Characterization

CHAPTER- II

SYNTHESIS AND CHACTERIZATION

PART - A

SYNTHESIS OF FERRITES

2.A.1 Introduction

A number of techniques both physical and chemical, have been developed to prepare nano sized magnetic particles.

The properties of ferrites are very much sensitive to the preparation conditions and are highly influenced by heat treatment, crystal structure and cation distribution. The porosity, density, grain size and orientation of grains etc. are important factors, which affect the properties of the ferrite materials. The other factors such as purity of material, stoichiometry and chemical homogeneity also affect ferrite properties.

The nanocrystalline preparation methods for materials are broadly classified as

1. Physical
2. Chemical
3. Biological

2.A.2 Physical methods

2.A.2.a Melt spinning

The two phase materials of a hard magnetic phase coupled to a soft one are prepared by this method. In this method the starting materials consists of three to five elements, which on heating in some inert atmosphere give an alloy ingot. This ingot is then crushed into small pieces for melt spinning. The melt spin amorphous samples with various thicknesses are prepared by using single roll melt spinning equipment. The amorphous samples have to be sealed in an evacuated quartz tube and annealed for various periods [1]. This method has a minimal interface contamination and can produce almost pore free samples.

2.A.2.b High-energy ball milling

This method is used for the preparation of nanocrystalline alloys. Some times this method is referred to as mechanical alloying or mechanical milling. The size of the nanoparticles depends on several factors viz. milling speed, type, size, distribution of balls, ball to powder weight ratio, milling atmosphere etc [2]. This process has the advantage that we can produce large quantities of material.

2.A.2.c Sputtering

This method involves acceleration of ions of elements like argon or krypton to high energies and their bombardment into target materials. Various sputtering parameters like environment, its pressure, sputtering

power, duration and also annealing can be used to achieve the grain size [3, 4]

2.A.2.d Glass ceramic method

In this method glass-ceramics are produced by controlled crystallization of appropriate glasses. The glass specimens are subjected to heat treatment at nucleation and crystallization temperature respectively. Crystallization temperature is determined from differential thermal analysis (DTA) [5].

2.A.2.e Molecular beam epitaxy

In this method epitaxial layers are grown on a heated substrate by impinging molecular or atomic beams evaporated from sources under ultra high vacuum conditions. In this method the source and the substrate temperature are separately controlled to achieve epitaxial growth [6].

2.A.3 Chemical methods

2.A.3.a Sol-gel route

This method involves the formation of amorphous network as distinct from a crystallization process [7]. This process involves formation of an amorphous gel from solution through hydrolysis and polycondensation reaction. The gelation takes places in nearly forty eight hours. It is then sintered for different periods of time to obtain nanocrystalline ferrite.

2.A.3.b Co-precipitation route

Precipitation of multi component system is known as co-precipitation. This process involves formation of a solid precipitate followed by the separation of the solid within a filtration step. This process needs a co-precipitation agent. The parameters like mixing rate, pH, temperature, concentration etc. have to properly adjusted [8].

2.A.3.c Micro emulsion technique

Nanocrystalline ferrites based on the reverse micelle concept may be synthesized using two micro emulsions systems. First micro emulsion system is an oil-phase micro emulsion comprising of isooctane and surfactant octylsulf- occinate and second is an aqueous phase emulsion consisting of isooctane. This process is performed in restricted environment [9].

2.A.3.d Glyoxylate precursor method

The hetropolynuclear complex combination of Fe^{3+} and divalent metal cations is used as a precursor for preparing the ferrite [10]. This synthesis consists in the mixing of 1, 2 – ethanediol (ethylene glycol) (Fluka) with nitrates.

2.A.4 Biological method

Metal based nanocrystalline ferrites are being investigated by the biological method or those that attempt to mimic biological methods. Generally these biological methods rely on the process of boimeriralization [11-13].

2.A.5 Fast Firing method (Paramanik Method)

Stoichiometric amounts of the metal nitrates are thoroughly mixed in accordance with proper composition. 10% PVA and aqueous solution of sucrose are mixed together while stirring with a magnetic stirrer. The resulting solution is heated at 200^0C. The complete NO_2 evaporation takes place with the formation of the highly viscous liquid. Further heating of the liquid causes decomposition to a voluminous organic based black, fluffy mass, which is ground to a fine powder to form the precursor material. Heat treatment of the precursor material results in the formation of desired nanocrystalline magnetic oxide materials.

2.A.6 Role of Sucrose

In fast firing method, sucrose provides a wrapping through co-ordination for the cations in solution and circumvents their selective precipitation from the solution during the evaporation process. The excess of sucrose on the solution of metal ions, work as a chelating agent and ensures atomistical distribution of the cations throughout the polymeric network structure.

$$C_{12}H_{12}O_{11} + M(NO_3)_x + C\,CH(OH)\text{-}(H_2)_n \rightarrow C + M_2O_x + NO_2 \quad \text{----2.1}$$

The sucrose solution also provides the efficient fuel to combustion reaction being oxidized by the nitrate ions. Stability of the polymeric approach is because of the chemical bonding of the cations on to polymeric chain and from the high viscosity polymeric solution. The chemical bonding

is destroyed during the pyrolysis the h gh viscous favors low cation mobility which helps to affect the crystalline morphology.

When the aqueous solution of sucrose is mixed with nitrate, sucrose gets hydrolyzed to gluconic acid and polyhydroxy acid. The gluconic acid has a carboxylic acid group and fixed l near hydroxy groups. Because of this, it can participate into the metal ions and from a polymer chain with PVA.

The PVA solution provides polymeric matrix structure and also provides heat for combustion of carbonaceous materials. It also helps in polycondensaton reaction in the presence of oxidized saccharides and gives rise the polymer network structure, where the metal on (M^{2+}) are held in the hydroxylic pockets of the branch chain through complex fraction.

The polymer chain with PVA and metal ions provides wrapping for the cations in solution.

2.A.7 Actual method of ferrite samples

i. Preparation of 10 % PVA solution

To prepare 10% PVA (Polyvinyl alcohol) solution, 20 gm of solid PVA was dissolved in 200 ml of double distilled water. The mixture was stirred with the help of a magnetic stirrer for half an hour at 80 ^{0}C to get a clean solution.

The 30 gm sucrose and 10 ml of 10% PVA solution were mixed with 50 ml double distilled water is added.

Appropriate quantities of metal nitrates were dissolved in 50 ml double distilled water to get a homogeneous solution. A mixture containing 30 gm sucrose and 10 ml of adequate 10% PVA solution mixed with 50 ml double distilled water is added. The resultant mixture is stirred with the help of a magnetic stirrer at 80 °C for an hr.

During heating at 80 °C NO_2 fumes are released and a viscous mixture is formed. The viscous mixture is transferred to a beaker and continuously heated. The evaporation process takes place and lastly the powder burns like live charcoal. After completion of the oxidation process the ferrite powder is formed.

The ferrite samples with the general formula $Li_{0.5}Ni_{1.5x}Fe_{2.5-x}O_4$ with (x = 0.1, 0.2, 0.3, 0.4, 0.5) were prepared using this method. All the samples were presintered at 800 °C for 8 hr in air.

The presintered powders were subjected to hand milling and sieved. The pellets of 1.5 cm diameter and 2-3 mm thickness were prepared by pressing the powder with the help of a hydraulic press applying a pressure of about 5 tons per square inch for 5 to 10 minutes. The pellets were subjected to final sintering at 900 °C for 12 hr in air.

PART - B

STRUCTURAL CHARACTERIZATION

2.B.1 Introduction

. For the structural study of ferrites x-ray diffraction is one of the powerful tools. The confirmation of spinel phase of ferrites and completion of solid state reaction can be studied by this technique.

The x-ray diffraction maxima occurs when the Bragg's condition,

$$2d \sin\theta = n\lambda \qquad \text{----- 2.2}$$

where n = order of the diffraction

λ = wavelength of monochromatic x-rays

ϕ = interplaner distance

θ = glancing angle

is satisfied.

The schematic diagram of x-ray diffractometer is shown in Fig. 2.B.1.

2.B.2 X-ray diffraction technique.

The different methods of X-ray diffraction methods [14, 15] are Laue method, rotating crystal method and pcwder method. The powder method is the most suitable method for polycrystalline samples.

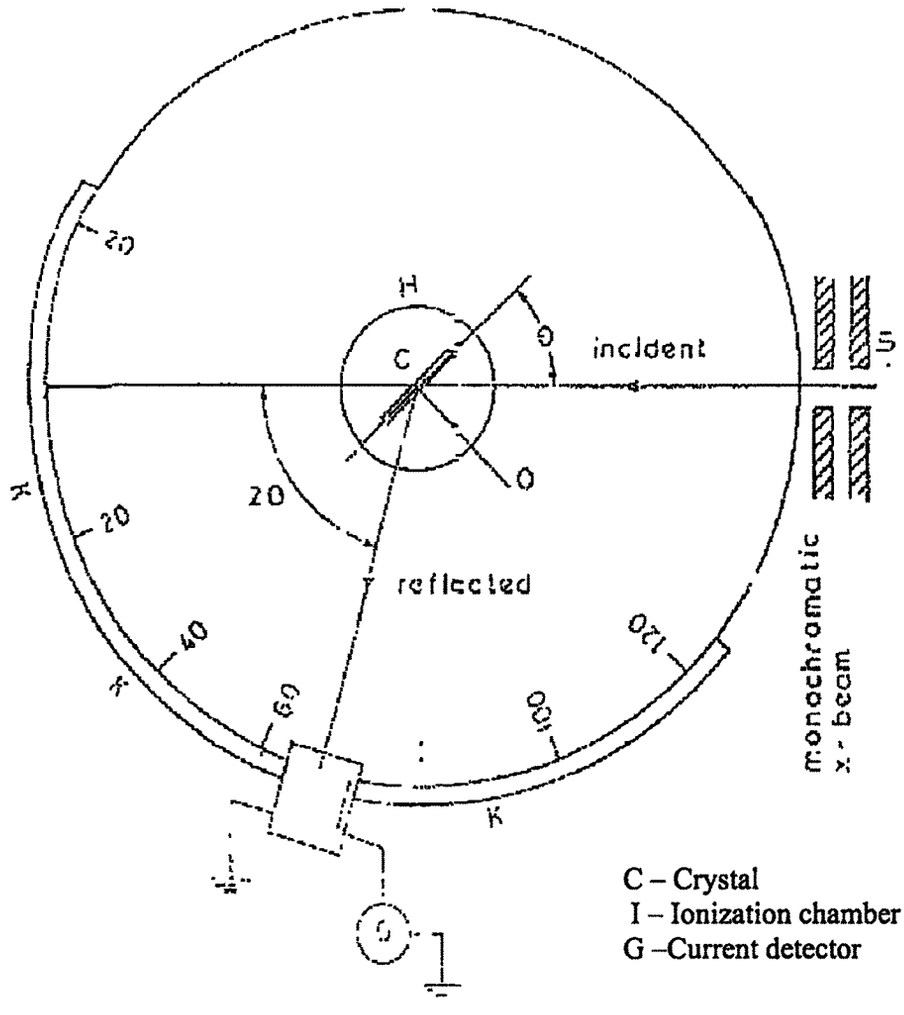

Fig. 2.B.1 - Schematic diagram of X-ray diffractometer

The Powder method was developed by Debye and Scherrer [14]and Hull [15]independently. Very fine powder of the sample is rotated in a beam of monochromatic x-ray. Each particle of powder is a tiny crystal oriented at random. Krishnamurthy has used this method to find the cation distribution of Ni-Zn ferrites [16].

2.B.3 Experimental techniques

In the present case, x-ray diffraction patterns were obtained using x-ray diffractometer (Philips, Model PW 1710) using filtered Cu Kα radiation (λ = 1.5418 Å) at CFC, Shivaji University, Kolhapur. The diffraction patterns were takes in the 2θ range of 20° to 80°.

In case of cubic system the interplaner distance is given by -

$$d = \frac{a}{\left(h^2 + k^2 + l^2\right)^{1/2}} \qquad \text{---- 2.3}$$

where a = lattice parameter and

(h k l)=Miller indices

From equations (2.1) and (2.2) the lattice parameter can be expressed as

$$a = \frac{\lambda}{2.Sin\theta} \times \left(h^2 + k^2 + l^2\right)^{1/2} \qquad \text{---- 2.4}$$

for first order diffraction,

The prominent line in the diffraction pattern of the spinels corresponds to (311) plane. The value of diffraction angle (θ) corresponding to (311) plane is noted from the diffraction pattern.

Substituting the values of sin θ, (311) and λ in equation 2.3, lattice parameter 'a' was calculated. With the lattice parameter 'a', the indices and'd' values for other planes were calculated by usual procedure. The planes that diffract x-ray in the cubic spinel structure are (111), (220), (311), (222), (400), (333), (440).

The diffractograms were indexed with the help of ASTM data available for spinel ferrites. The interplaner distances were also calculated. The bond lengths R_A and R_B were calculated by the relations,

$$R_A = a3^{1/2}\left(\delta + \tfrac{1}{8}\right) \qquad \text{---- 2.5}$$

$$R_B = a\left(3\delta^2 + \frac{1}{16} - \frac{\delta}{2}\right)^{1/2} \qquad \text{---- 2.6}$$

where $\delta = u\text{-}u_{ideal}$, $u_{ideal} = 0.375$

$u = (u_1 + u_2)/2$

$u_1 = 0.381$ A for $Ni\ Fe_2O_4$

$u_2 = 0.380$ A for $Li_{0.5}Fe_{2.5}O_4$

The site radii were calculated using the relations

$$r_A = a3^{1/2}\left(u - \frac{1}{4}\right) - r_o \qquad \text{---- 2.7}$$

$$r_B = a\left(\frac{5}{8} - u\right) r_o \qquad \text{---- 2.8}$$

where r_o =1.35 Å (radius of oxygen ions)

2.B.4 Results and discussion

X-ray diffraction pattern of the samples $Li_{0.5}Ni_{1.5x}Fe_{2.5-x}O_4$ (where x = 0.1, 0.2, 0.3, 0.4, 0.5) are shown in Fig 2.B.2 to 2.B.3

The diffraction peaks (220), (311), (222), (400), (422), (333), (440) are observed. For the spinel ferrites the (311) peak is more intense. All the samples exhibit cubic spinel structure No extra lines were observed in the present case, which confirms that, the single phase spinel ferrites are formed. The inter planer distances were calculated for different diffraction lines. The observed and calculated'd' values are given in Table 2.1 to 2.5. It is seen that the observed and calculated'd 'values are good in agreement. The cyclic sum of Miller indices viz. (h +k), (k + l), (l – h) is an even integer. It concludes the face centered cubic structure of the ferrites. The lattice parameters were calculated using the equation 2.3. Fig. 2.B.4 shows the variation of lattice parameter with Ni^{2+} content.

The increase of lattice parameter 'a' with Ni^{2+}content up to x =0.3 can be explained on the basis of ionic size difference of component ions. The Ni^{2+} ions have larger ionic radius (0.78 Å) than Fe^{3+} (0.65 Å). The Ni^{2+} ions successively replace the Fe^{3+} ions on the A site. For Ni^{2+} content of x =0.4 and 0.5, the lattice parameter decreases due to the smaller ionic radius of Li^{1+} (0.71 Å). The values of lattice parameters lie in the range of 8.26 to 8.33 Å. Krishna et al. [17] have been reported the value of 'a' to be 8.330 Å of Li-

ferrite. The value of 'a' for Li –ferrite has been reported to be 8.382 Å by Naik (18).

The data on bond length (R_A and R_B) and site radii (r_A and r_B) with the Ni^{2+} content is given in the Table 2.6. Fig. 2.B.5 shows the variation of (R_A and R_B) with the Ni^{2+} content. From this figure, it is observed that the bond length R_A and R_B decreases with the composition x =0.4 and 0.5 which can be attributed to the variation in lattice parameter with Ni^{2+} content. The R_B is greater than R_A

Fig. 2.B.6 shows the variation of site radii r_A and r_B with the composition. From figure it is observed that site radii also increase with nickel content. The variation of site radii is similar to the variation of bond lengths. r_A is less than r_B .

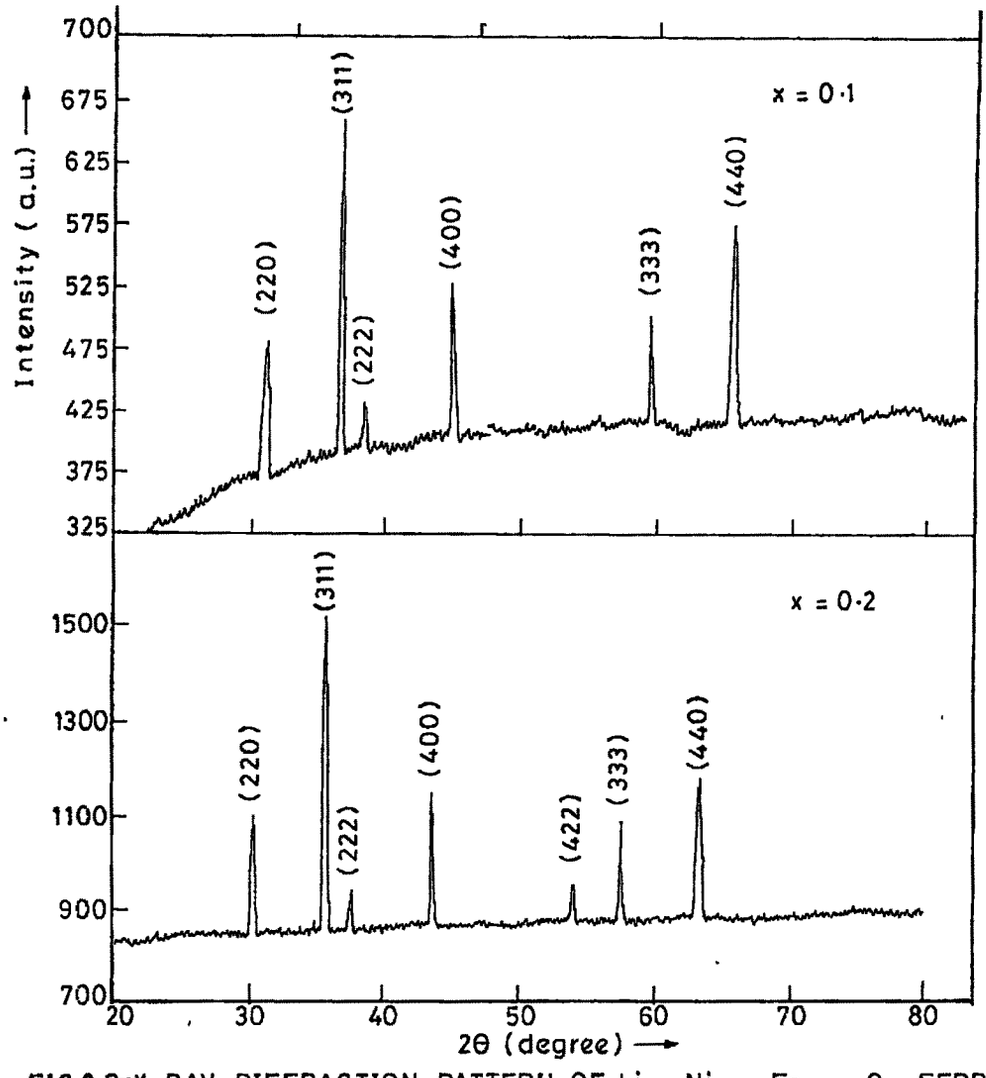

FIG.2.8 X-RAY DIFFRACTION PATTERN OF $Li_{0.5}Ni_{1.5-x}Fe_{2.5-x}O_4$ FERRITES

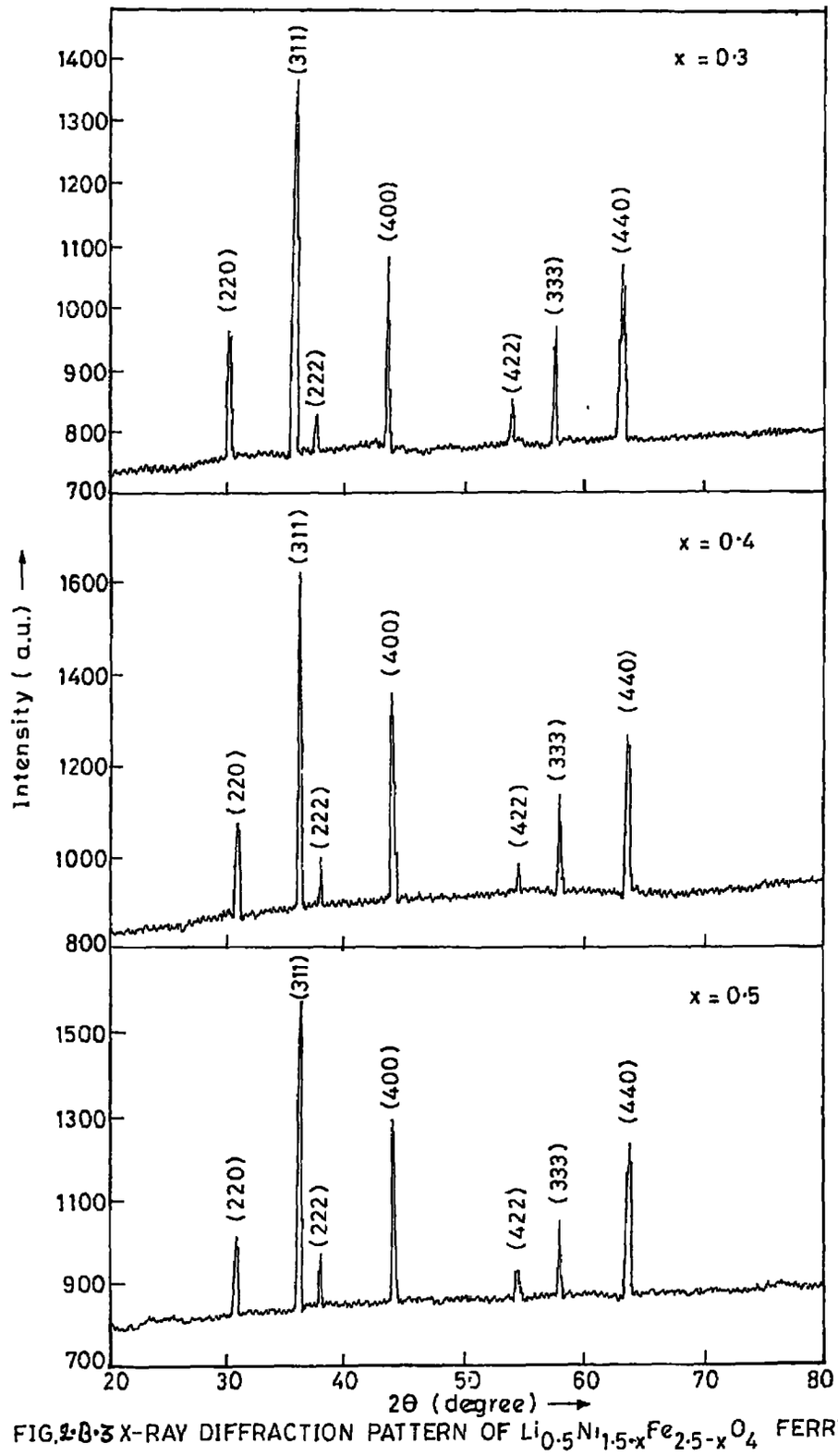

FIG. 2·B·3 X-RAY DIFFRACTION PATTERN OF $Li_{0.5}Ni_{1.5-x}Fe_{2.5-x}O_4$ FERRITES

Table 2.1 - X-ray diffraction data of $Li_{0.5}Ni_{0.15}Fe_{2.4}O_4$ ferrite

$\lambda = 1.5418$ Å a = 8.293 Å

Sr.No.	2θ	θ	Sin θ	$d_{obs.}$	$d_{cal.}$	hkl
1	30.49	15.245	0.262	2.929	2.931	(220)
2	35.885	17.943	0.308	2.500	2.502	(311)
3	37.625	18.81	0.322	2.389	2.394	(222)
4	43.650	21.83	0.373	2.072	2.072	(400)
5	57.57	28.79	0.482	1.599	1.599	(333)
6	63.315	31.66	0.525	1.4680	1.468	(440)

Table 2.2 - X-ray diffraction data of $Li_{0.5}Ni_{0.3}Fe_{2.3}O_4$ ferrite

$\lambda = 1.5418$ Å a = 8.312 Å

Sr.No.	2θ	θ	Sin θ	$d_{obs.}$	$d_{cal.}$	hkl
1	30.370	15.185	0.252	2.940	2.942	(220)
2	35.800	17.9	0.307	2.506	2.511	(311)
3	37.515	18.76	0.322	2.396	2.394	(222)
4	43.595	21.798	0.371	2.075	2.077	(400)
5	53.945	26.973	0.454	1.698	1.698	(422)
6	57.485	28.743	0.481	1.602	1.602	(333)
7	63.315	31.66	0.525	1.468	1.468	(440)

Table 2.3 - X-ray diffraction data of $Li_{0.5}Ni_{0.45}Fe_{2.2}O_4$ ferrite

$\lambda = 1.5418$ Å a = 8.328 Å

Sr.No.	2θ	θ	Sinθ	$d_{obs.}$	$d_{cal.}$	hkl
1	30.355	15.178	0.262	2.942	2.942	(220)
2	35.730	17.865	0.307	2.511	2.511	(311)
3	37.485	18.743	0.321	2.397	2.397	(222)
4	43.530	21.770	0.371	2.077	2.077	(400)
5	53.920	26.960	0.453	1.699	1.699	(422)
6	57.445	28.723	0.481	1.603	1.602	(333)
7	63.255	31.628	0.524	1.469	1.471	(440)

Table 2.4 - X-ray diffraction data of $Li_{0.5}Ni_{0.60}Fe_{2.1}O_4$ ferrite

$\lambda = 1.5418$ Å a = 8.289 Å

Sr.No.	2θ	θ	Sinθ	$d_{obs.}$	$d_{cal.}$	hkl
1	30.500	15.25	0.263	2.929	2.9231	(220)
2	35.900	17.95	0.308	2.499	2.499	(311)
3	37.620	18.81	0.322	2.389	2.394	(222)
4	43.685	21.84	0.372	2.070	2.072	(400)
5	54.015	27.01	0.454	1.696	1.698	(422)
6	57.750	28.88	0.483	1.595	1.596	(333)
7	63.380	31.69	0.525	1.466	1.468	(440)

Table 2.5 - X-ray diffraction data of $Li_{0.5}Ni_{0.75}Fe_2O_4$ ferrite

$\lambda = 1.5418$ Å a = 8.258 Å

Sr.No.	2θ	θ	Sinθ	$d_{obs.}$	$d_{cal.}$	hkl
1	30.485	15.243	0.263	2.929	2.931	(220)
2	36.055	18.027	0.315	2.502	2.490	(311)
3	37.540	18.770	0.322	2.394	2.394	(222)
4	43.635	21.818	0.372	2.073	2.072	(400)
5	53.960	26.980	0.454	1.698	1.698	(422)
6	57.515	28.760	0.481	1.601	1.602	(333)
7	63.335	31.670	0.525	1.467	1.468	(440)

Table 2.6 - Data on lattice parameter, bond length (R_A, R_B) and Site radii (r_A,r_B)

x	Lattice parameters	R_A (Å)	R_B (Å)	r_A (Å)	r_B (Å)
0.1	8.293	1.874	2.028	0.524	0.677
0.2	8.312	1.878	2.033	0.528	0.682
0.3	8.328	1.882	2.037	0.532	0.686
0.4	8.289	1.873	2.027	0.523	0.676
0.5	8.258	1.875	2.030	0.525	0.679

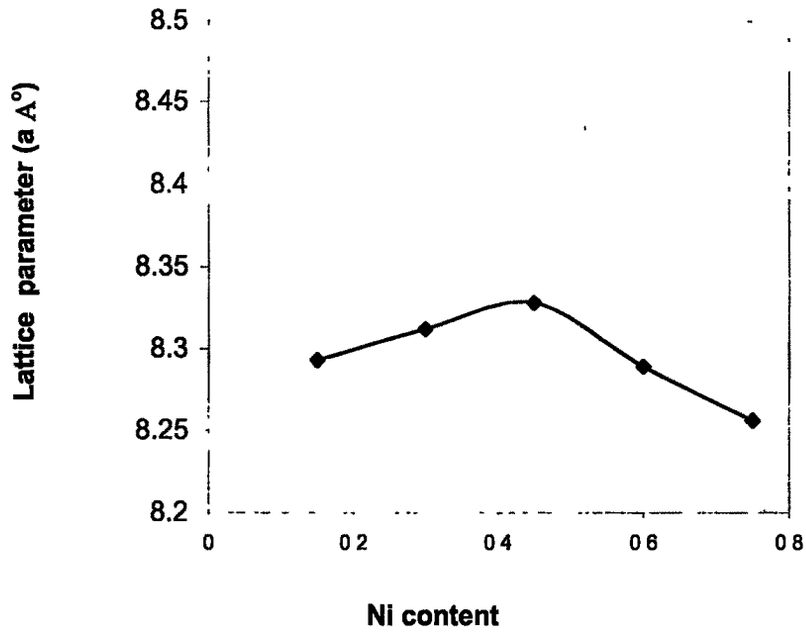

Fig. 2.B.4 - Variation of lattice parameterwith Ni^{2+} content

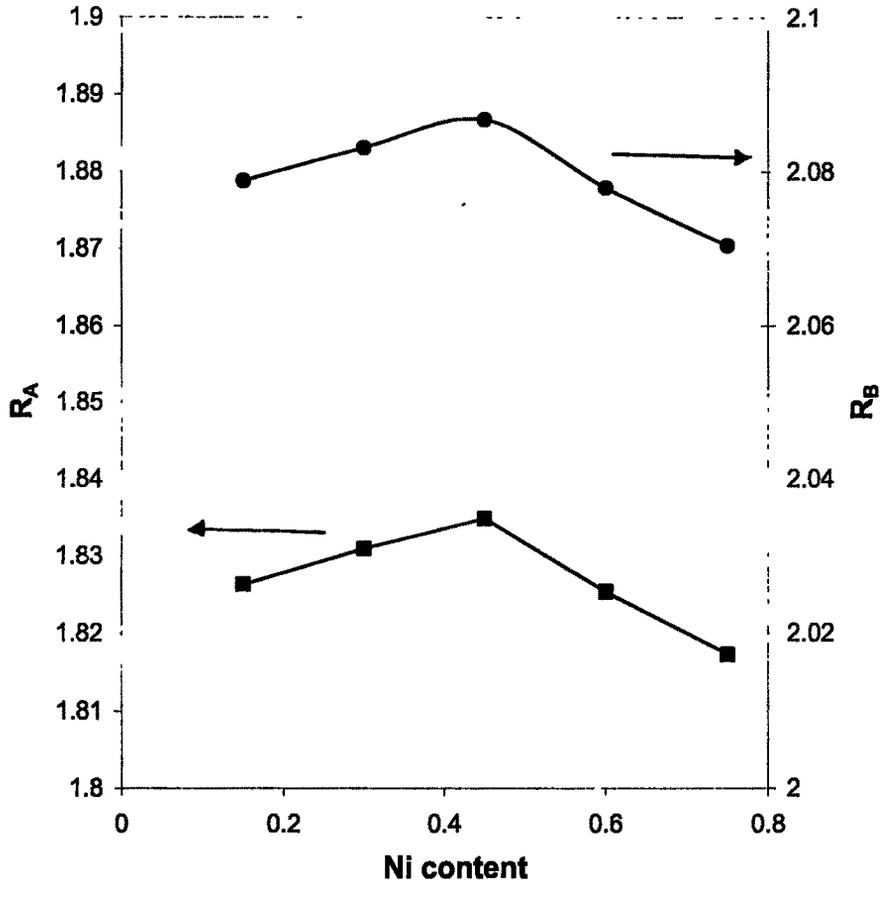

Fig. 2.B.5 - Variation of R_A and R_B with Ni^{2+} content

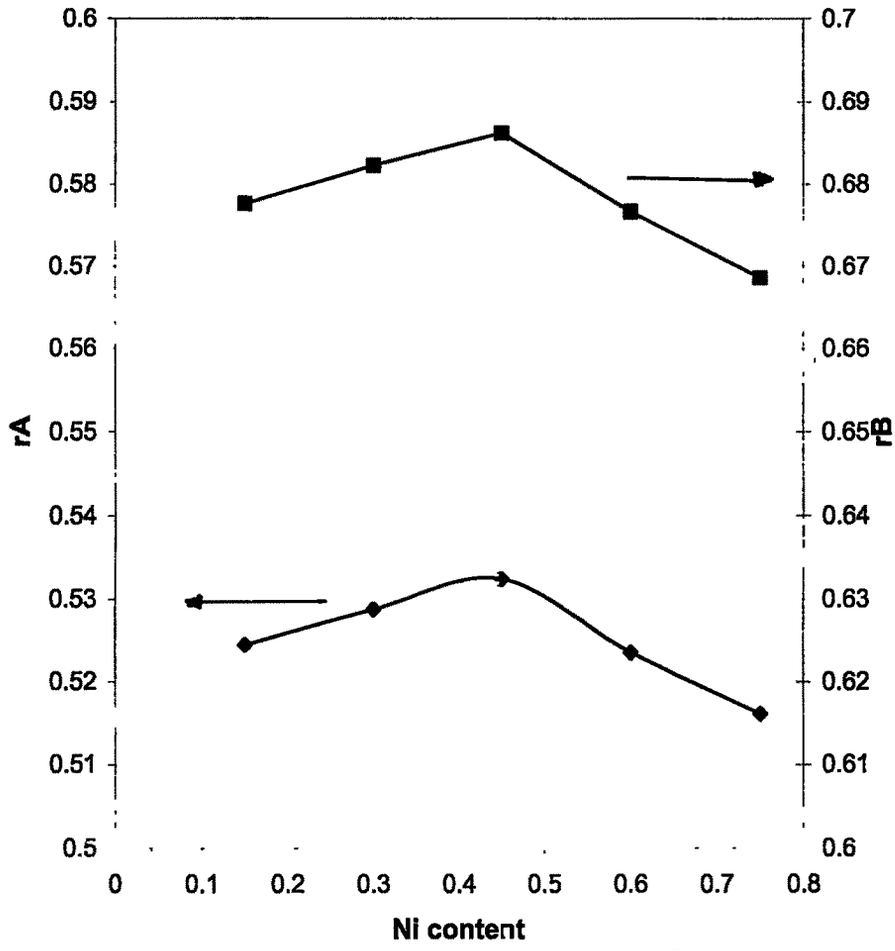

Fig. 2.B.6 - Variation of rA and rB with Ni^{2+} content

PART C

SCANNING ELECTRON MICROSCOPY

2.C.1 Introduction

Microstructure of the ferrites plays an important role in controlling their properties. The properties of ferrites such as permeability, magnetic loss, hystersis loop etc are microstructure dependent [19]. However some properties like saturation magnetization, magnetostriction, Curie temperature, are known as intrinsic properties while permeability, hysteresis etc. are the structure sensitive properties [20].

The scanning electron microscopy has been the most important technique for the study of microstructure of ferrites. It possesses high resolving power, high magnification and can produce three dimensional images.

2.C.2 Microstructure

In order to obtain the optimal properties of ferrites, it is essential to have the knowledge of their microstructural characteristics. For polycrystalline ferrites the microstructure includes porosity, grain size and phase structure. The sintering process helps in the development of final structure [21].

2.C.3 Sintering

Sintering consists of heating the compact to a significant temperature. For the same final density, the sintering temperatures are significantly lower for nanocrystalline ferrites, as compared to those for conventionally prepared ferrite powders. The achievement of very fine grained microstructures simultaneous with high densities is difficult. At a density of about 60% the grains begin to grow in volume by sweeping the pores. The pores within the grains are later on removed by the diffusion of vacancies to the grain boundaries. The sintering temperature plays the crucial role for the sample porosity.

The formation of ferrites is due to the counter diffusion mechanism of cations through the relatively high rigid oxygen lattice [22].

2.C.4 Porosity and grain growth

Porosity is the particle size depending factor of the structure of ferrite. Increasing the sintering rate lowers the porosity. Electrical properties of ferrites depend on the grain size and porosity. Large pores grow at the expense of the small pores by grain boundary diffusion of vacancies.

When the average grain size reaches its critical size the exaggerated grain growth occurs. It is due to the rapid growth of few grains. The rapid grain growth entraps pores within the matrix and it is almost impossible to eliminate such pores due to their greater distance from the grain boundaries. At the time of grain growth, grain boundaries move towards their center of

curvature. When the pores or inclusions disappear during heating, a somewhat large grain is formed in the matrix. The grain growth occurs when the following condition is satisfied.

$$D_{cr} = di/d_{fi} \qquad \text{---- 2.8}$$

where , D_{cr} - critical diameter of the grain

di - diameter of the inclusion

d_{fi} - Volume fraction of inclusion

When the grain size reaches this dimension, further grain growth is inhibited.

However very small pores are found to move along with moving grain boundary due to vacancy gradient over the two pore surfaces [23]. The optimum sintering rate is achieved when the following condition is satisfied

$$D_c C_c = D_o C_o \qquad \text{---- 2.9}$$

where D_c – diffusion constant of cation vacancies

D_o – diffusion constant of oxygen vacancies

C_c – Bulk concentration of the cation vacancies

C_o – Bulk concentration of the oxygen vacancies

Combination of small grain and low porosity is extremely difficult to realize in practice. At higher sintering rate lower pore growth becomes predominant and it is difficult to reduce the grain size.

The grain growth mechanism is compromise between driving force for boundary movement and retarding force of pores and inclusions during

the sintering process. The strength of the driving force, generates due to thermal energy, depends upon sintering temperature and diffusivity of constituent ions. The mechanism of neck growth as a consequence of migration of vacancies from pores to grain boundry is observed in a micrograph. The samples shows fine grains with small sized inclusions spread between them.

2.C.5 Literature survey

SEM technique determines the grain size and variation of grain size with doping concentrations. Not only the size of the particles, but the uniformality of ferrite particles can be studied with SEM. The spherical grains 200-400 nm in diameter are reported by Caruntu et al. [24]. They have prepared nickel ferrite thin films on glass and silicon substrate. Tang et al. [25] have studied the effect of annealing on the magnetic properties of nanocrystalline $ZnFe_2O_4$ and reported the particle size of about 3 nm.

Bhosale [26] carried out SEM studies on $Cu_{0.1}Mg_{0.4}Zn_{0.5}Fe_2O_4$ on initially sintered and then hot pressed samples.

Formation of nanocrystalline thin films of zinc ferrite with varying Zn^{2+} concentration on glass substrate was confirmed by SEM [27]. SEM photographs of the sintered Ni–Zn ferrite samples prepared by microwave-assisted flash combustion technique are also reported earlier [28].

Ravindranathan et al. [29] have carried out SEM studies of $Ni_{0.5}Zn_{0.5}Fe_2O_4$ ferrite prepared at 1000 °C. SEM micrographs studies on high permeability of Mn-Zn ferrite have been reported [30].

SEM micrographs of basic composition of, $Cu_{0.162}Fe_{0.054}Zn_{0.405}Mg_{0.405}Fe_{1.892}O_4$ prepared at 1045 °C and $Cu_{0.162}Fe_{0.054}Zn_{0.325}Mg_{0.325}Ni_{0.162}Fe_{1.892}O_4$ at sintered at 1035 °C have been reported [31]. Bhosale [32] has observed decrease in grain growth in Gd substituted Mg-Cd ferrite. Many other researchers have reported similar SEM studies earlier [33, 34 and 35]. Ghodake [36] investigated the substitution of nickel in Cu-Zn ferrite. It was found that with the addition of Ni^{2+} the average grain diameter went on changing and there was no relation between average grain diameter and content.

2.C.6 Experimental techniques

The SEM micrographs of the sample in the present work were obtained from the Department of Physics, Shivaji University, Kolhapur using SEM (Model JEOL – JSM 6360).

2.C.7 Results and discussion

The SEM micrographs of the samples in the present case are presented in Fig.2.C.1 to 2.C.3. The average grain diameter was calculated using line intercept method and given in Table 2.7. It is observed that as Ni content in the sample increases the grain size decreases and the porosity of the sample increases. It is observed that the values of grain diameter are in

the range of 175 nm to 109 nm. The grain boundaries are distinct and grains are closely packed suggesting that the material has high density and exhibits high magnetization.

Lack of chemical homogeneity as well as variation in density and presence of impurities favor exaggerated grain growth [37]. Beck et al. [38] have shown that exaggerated grain growth could be associated with the disappearance of inclusion by solution. The micrographs clearly include such behavior.

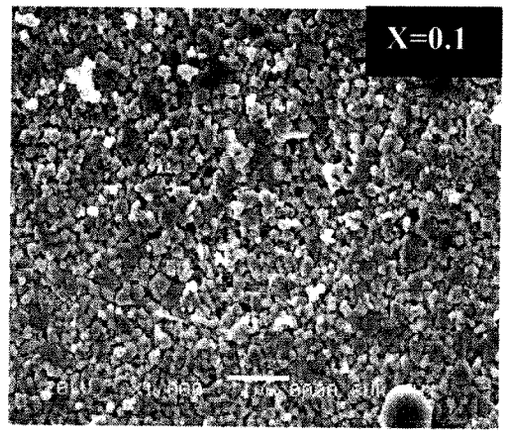

Fig. 2.C.1 SEM micrographs for $Li_{0.5}Ni_{0.15}Fe_{2.4}O_4$ ferrite

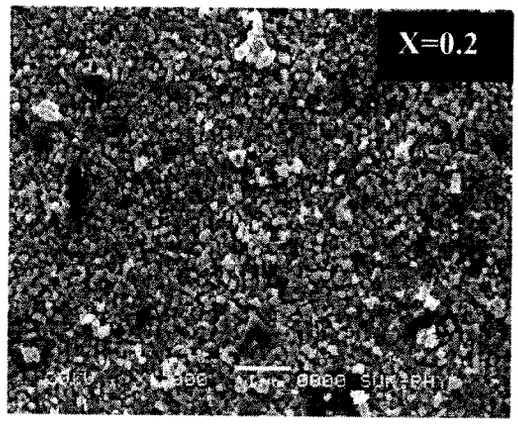

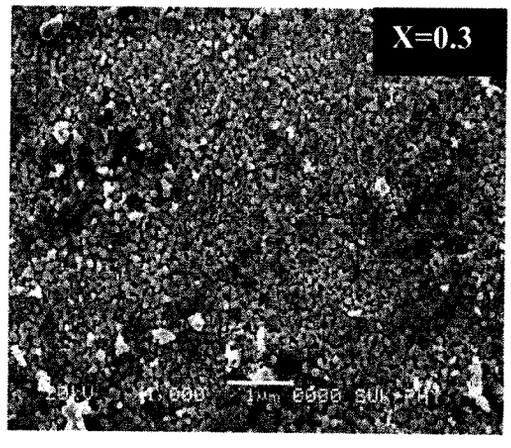

Fig. 2.C.2 SEM micrographs for $Li_{0.5}Ni_{1.5x}Fe_{2.5-x}O_4$ ferrites

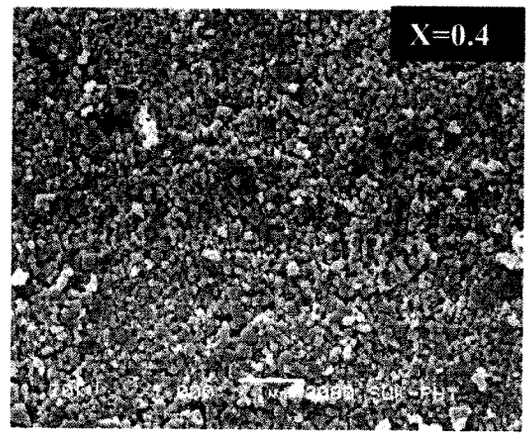

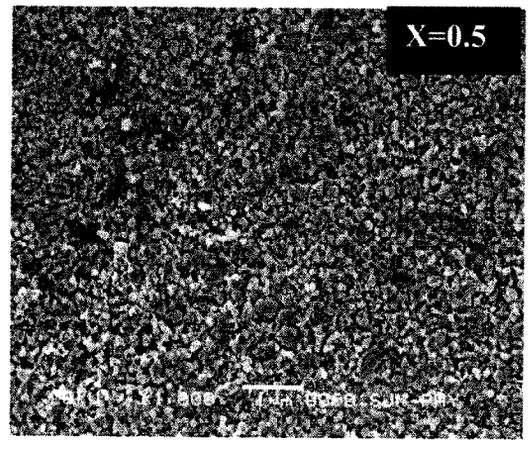

Fig. 2.C.3 SEM micrographs for $Li_{0.5}Ni_{1.5x}Fe_{2.5-x}O_4$ ferrites

Table 2.7-Data on grain size and porosity for $Li_{0.5}Ni_{1.5x}Fe_{2.5-x}O_4$ ferrite samples

X	Grain size (nm)	Porosity (%)
0.1	175	18
0.2	156	19
0.3	122	21
0.4	120	22
0.5	109	23

PART D

INFRARED ABSORBTION

2.D.1 Introduction

Infrared spectroscopy is used

(i) to determine local symmetries in crystalline and non-crystalline solids and ordering phenomena in spinels.

(ii) to determine the vibrational energy of molecules in solids. Infrared spectroscopy is used to detect the completion of solid state reaction, study of cation distribution, deformation of spinel structure of the ferrites,

(iii) to calculate the force constants for tetrahedral and octahedral sites.

Waldron [39] was the first to study the infrared spectra of ferrites in a systematic manner. He reported four infrared active fundamentals in the vibrational spectra of normal and inverse spinel ferrites in the frequency range of 200 to 800 cm^{-1}. The absorption bands in the spinel ferrites mainly arise from vibrations of oxygen ions with cations producing various frequencies of the unit cell. The frequencies of vibrations depend on cation mass, unit cell parameter and cation oxygen bonding in complex manner.

Spinel ferrites usually show two absorption bands corresponding to tetrahedral and octahedral sites. The high frequency band υ_1 is ascribed to tetrahedral complexes and low frequency band υ_2 to octahedral complexes. Waldron [3] has given the detail procedure for the computation of force constants and specific heat of the materials.

2.D.2 Experimental techniques

The IR spectra of the $Li_{0.5}Ni_{1.5x}Fe_{2.5-x}O_4$ ferrite samples in the present work were obtained from CFC, Shivaji University, Kolhapur using the Perkin Elmer IR spectrometer (model 783) in KBr medium in the frequency range 200 to 800 cm^{-1}.

2.D.3 Results and discussion

The IR absorption spectra of the samples in the system $Li_{0.5}Ni_{1.5x}Fe_{2.5-x}O_4$ (where x = 0.1, 0.2, 0.3, 0.4, 0.5) are shown in Fig.2. D.1 and 2.D.2. Table 2.8 gives the data on absorption bands along with their wave numbers. In the present work it has been found that the vibrations $\upsilon_1$and υ_2 bands are around 600 cm^{-1} and 400 cm^{-1} respectively. Splitting of principal bands have been attributed to Jahn-Teller distortion in the lattice produced by Fe^{2+} ions which locally produces deformation in the lattice.

Waldron has attributed the band υ_1 around 600 cm^{-1} to the vibrations of tetrahedral complexes corresponding to the highest restoring force where as band υ_2 around 400 cm^{-1} is attributed to vibrations of octahedral

complexes which are bond bending vibrations. Therefore it is reported that υ_1 is greater than υ_2. Hafner [40] and White and Angelish [41] have reported IR studies of ferrites. Their results support the Waltron's results.

The IR spectrum of pure lithium ferrite has been found to be similar to that of the ordered spinels. As the concentration of Ni^{2+} ions is increased in lithium ferrite, Ni^{2+} ions having strong preference for octahedral site replace Fe^{3+} ions of comparable mass and radii. Hence it is expected that IR spectra should not be influenced by random distribution of Fe^{3+} and Ni^{2+} ions in the lattice. Tarte and Prudhome [42,43] have reported that both υ_1 and υ_2 depend on the nature of octahedral cations but not on the nature of the tetrahedral cations. Navdeep and Puri [44] have studied IR spectra of Li-Cr ferrites [45].

It is observed that υ_1 goes on increasing with Ni^{2+}content and υ_2 are nearly constant with Ni^{2+}content. Kharabe et al. [46], Bellad [47] and Reddy [48] have reported similar results for low Ni^{2+} content and high Cd^{2+} content in lithium ferrite.

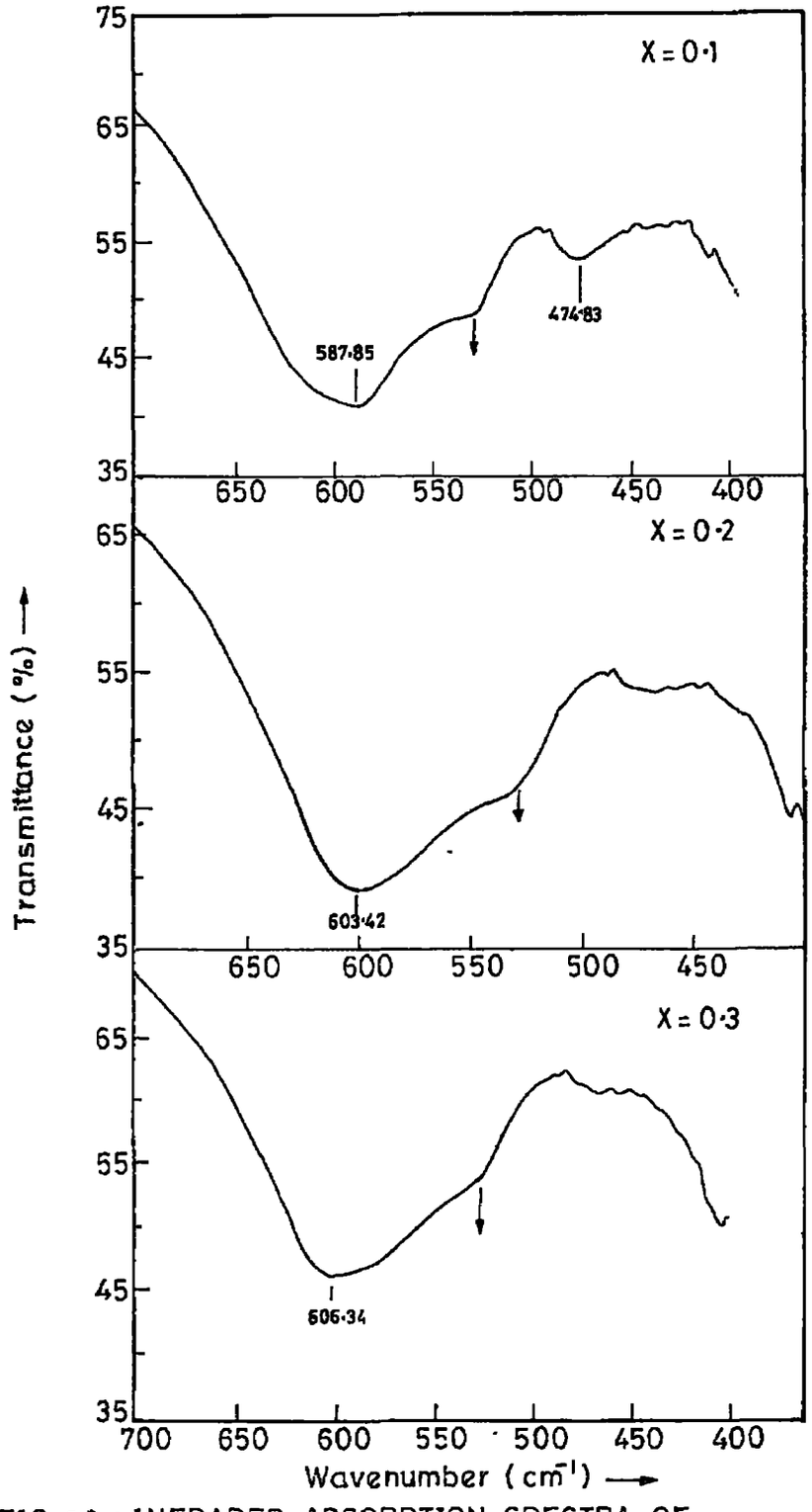

FIG.2·D·1 INFRARED ABSORPTION SPECTRA OF $Li_{0.5}Ni_{1.5-x}Fe_{2.5-x}O_4$ SAMPLES FOR X = 0·1, 0·2, 0·3.

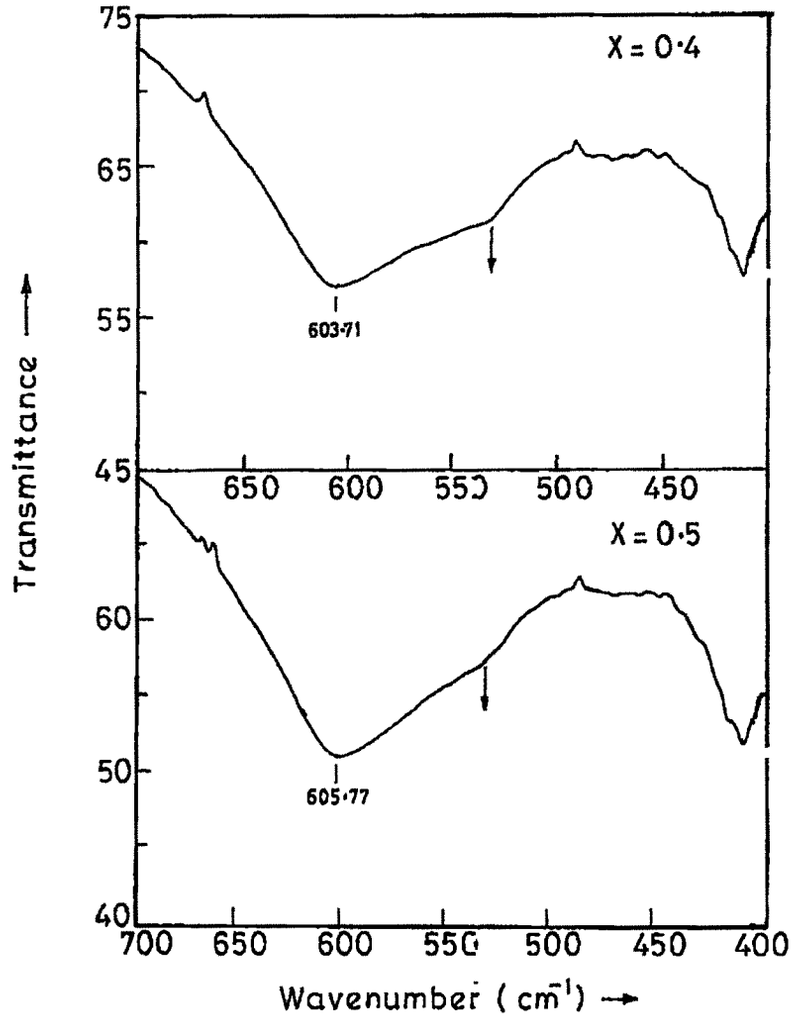

FIG.2·D·2 INFRARED ABSORPTION SPECTRA OF $Li_{0.5}Ni_{1.5-x}Fe_{2.5-x}O_4$ SAMPLES FOR X = 0·4, 0·5.

Table 2.8 - Absorption frequencies for the samples of $Li_{0.5}Ni_{1.5x}Fe_{2.5-x}O_4$ ferrites.

x	υ_1 cm^{-1}	υ_{1s} cm^{-1}	υ_2 cm^{-1}
0.1	587.85	527	410.85
0.2	603.42	529.28	409.92
0.3	606.34	533.47	409.92
0.4	603.71	532.55	410.85
0.5	605.77	527.78	410.85

References

1 D. H. Ping and K. Hono
J. Appl. Phys. 83 (1998) 7769-7775.

2 P.G. McCormick, W. F. Miao, P. A. I. Smith, J. Ding and R. Street
J. Appl. Phys. 83b (1998) 6256-6261

3 S. Stavroyianis, I. Panagitopoulos and D. Niarchos
Appl. Phys. Lett. 73 (1998) 3453-3455

4 S. Stavroyianis, I. Panagitopoulos and D. Niarchos
J. Appl. phys. 85 (1999) 4304-4306

5 M. Pal, P. Brahma, D. Chakravorty, D. Bhattacharyya and H. S. Maitti
Nanostruct. Mater. 8 (997) 731-738

6 N. Inoue, Y. Kawamura and K. Morimoto
"Handbook of Nanophase Materials"
New York, Marcel Dekker (1997) 83-140

7 R. Roy
Science 238 (1987) 1664-1669

8 M. Pal and D. Chakravorty
Sadhana 28 (1,2) (2003) 283-297

9 J. Chargles, N. O'Connor, E. Kolesnichenko, C. Carpenter, S. W. Zhou, A. Kumbhar, S. Jessica and A. Fabrice
Synthetic Metal.122 (2001) 547-555

10 M. Birzescu, M. Cristea, M. Stetanescu and G. H. Constantin
Rom. Pat. (1990) 1, 102501

11 C. T. Dameron, R. N. Resse, R. K. Mehra, A. R. Kkortan, P. J. Carroll, M. L. Steigerwold, L. F. Brus and D. R. Winge
Nature 338 (1989) 596

12 P. R. Smith, J. P. Holmes, D. J. Richardson, D. A. Russell and J. R. Socleau
J. Chem. Soc. Faraday Trans. 94 (1998) 1235

13 T. Torimoto, M. Yamashita, S. Kuwabata, T. Sakata, H. Mori and H. Yoneyama
J. Phys. Chem. B 103 (1999) 8799

14 P. Debye and P. Scherrer
Physica 17 (1916) 277

15 A.W. Hull
Phys. Rev. 9 (1916) 504

16 K. R. Krishnamurthy
Ph.D. Thesis, IIT Madras, India (1975)

17 P. Kishan, S. N. Chattterge, L.R. Nagpal and K.K. Laroia
Indian J. Pure and Appl. Phys. Vol. 19

18 A. B. Naik
Ph. D. Thesis, Shivaji Univ., Kolhapur (1993)

19 F. N. Bradley
"Material for Magnetic Function".
Hyden Book Co. Inc., D. B. Taraporewala and Sons Co. Pvt. Ltd. (1980) (2) 56

20 A. L. Stuijits
Proc. Int. Conf. on ferrites (1970) 1080

21 L. H. Van Vleck
"Ceramic microstructure"
West View, Boulder, Colarado (1976) 4

22 D. P. Elwell, R. Parker and Tinsley
Czech J. Phys. B – 17 (1967) 382

23 M. V. Speight and G. W. Green wood
Phil. Mag. 6 (1964) 683

24 G. Caruntut, I. Dumitru, G. G.Bush, D.Caruntu and C. J. O' Connor
J. Phys. D: Appl. Phys. 38 (2005) 811-8

25 L. D. Tang, V. Kolesnichenko, G. Caruntu, D. Caruntu, Y. Remond, V. O. Golub, C. J. O'Connor and L. Spinu.
Physica B 319 (2002) 116-121

26 D. N. Bhosale
Ph. D. Thesis, Shivaji Univ. ,Kolhapur(1997)

27 C. Gabriel, G. G. Bush and C. J. O'Connor
J. Mater. Chem. 14 (2004) 2753-2759

28 R.V.Mangalaraja, S. Ananthakumar, P. Manohar, F.D. Gnanam, M. Awano
Mater. Lett. 58 (2004) 1593-96

29 P. Ravindranathan and K. C. Patil
J. Mater. Sci. 22 (1987) 3261-3264

30 H. P. Peloschek and D. J. Perduijn
IEEE Trans. Magn. 4 (1968) 453-455

31 J. N. Koh and K. U. Kim
New Phys. (Korean Phys. Soc.) 26 (6) (1986) 540-549

32 J. L. Bhosale
Ph. D. Thesis, Shivaji Univ., Kolhapur (1994)

33 Z. Xing, Y. Z. Ji, L. Li, H. Zhang and Z. Gui.
J. Magn. Magn. Mater. 208 (2000) 55-60

34 T. Nakamura
J. Magn. and Magn. Mater. 168 (1997) 285-91

35 C.Y. Tsay, K. S. Liu, T. F. Lin and I. N. Lin
J. Magn. Magn. Mater. 209 (2000) 189-192

36 S.A Ghodake
Ph. D. Thesis, Shivaji Univ., Kolhapur (2001)

37 A. Hamelin and M. Paulus
J. Cryst. Growth 3 (1968) 163

38 P.A. Beck, M.C. Halzworth and P.Sperry
Trans. AMIE 180 (1949) 163

39 R. D. Waldron
Phys. Rev. 99 (1953) 1727

40 V. S. Z. Hafner
Z. Fur. Krist. 15(1961) 331

41 W. B. White and B. A. Angelis
Spetro. Chem. Acta.23 (a) (1967) 985

42 P. Tarte and R. Collongues
Ann. Chim. (France) 9 (1984) 135

43 J. Prudhome
Spectro. Chim. Acta 26 (A) (1970) 985

44 N. K. Gill and R. K. Puri
J. Pure Appl. Phys. A 23 (1985) 71-73

45 V. R. Potakora, N. D. Zverer and V. P. Romanov
Phys. Stat. Solid (a) 12 (1972) 623

46 R. G. Kharabe
Ph. D. Thesis, Shivaji Univ., Kolhapur (2000)

47 S. S. Bellad, R. B. Pujar and B. K. Chougule
Indian J. Pure Appl. Phys. 36 (1998) 598

48 P. V. Reddy and V. D. Reddy
J. Magn. Magn. Mater. 136 (1994) 279